DOI: 10.1021/ic900735n

Inorganic Chemistry
Article

# Ligand-Mediated Interconversion of Multiply-Interpenetrating Frameworks in $Cu^{I}/Re^{VII}$-Oxide Hybrids

**Haisheng Lin and Paul A. Maggard***

*Department of Chemistry, North Carolina State University, Raleigh North Carolina 27695-8204*

Received April 15, 2009

Two new copper(I)-rhenate(VII) hybrid solids, $Cu(bpy)ReO_4$ (**I**) and $Cu(bpy)_2ReO_4 \cdot 0.5H_2O$ (**II**) (bpy = 4,4′-bipyridine), with 2-fold and 4-fold interpenetrating networks, respectively, were prepared from hydrothermal reactions, and their structures characterized by single-crystal X-ray diffraction [**I**, *Pbca* (No. 61), $Z = 8$, $a = 10.8513(3)$ Å, $b = 12.9419(4)$ Å, $c = 15.6976(5)$ Å; **II**, $P\bar{1}$ (No. 2), $Z = 2$, $a = 11.8190(4)$ Å, $b = 12.6741(4)$ Å, $c = 13.7585(5)$ Å, $\alpha = 85.8653(13)^o$, $\beta = 81.6197(13)^o$, $\gamma = 84.0945(11)^o$]. The structure of **I** contains $6^3$ nets of neutral $CuReO_4$ layers that are pillared via bpy ligands on the Cu sites $\{CuO_3N_2\}$ to yield a 2-fold interpenetrating pillared-layered network. Conversely, the structure of **II** consists of a 4-fold interpenetrating diamond-type network with tetrahedral $\{CuN_4\}$ coordination nodes that are bridged by bpy ligands, with both $H_2O$ and $ReO_4^-$ within the pores. A surprising reversible structural interconversion between these two interpenetrating structures is possible via the insertion and removal of a single bpy ligand and $^1/_2H_2O$ per copper atom. The structural interconversion is accompanied by a change in color from yellow to red for **I** and **II**, respectively. Measured UV−vis diffuse reflectance spectra exhibit a significant red-shift in the absorption edge of ∼0.3 eV, with the optical bandgap size decreasing from ∼2.5 eV to ∼2.2 eV for **I** and **II**, respectively. X-ray photoelectron spectra and electronic structure calculations indicate that the valence band derived from the Cu 3d and N 2p orbitals in **II** are pushed higher in energy compared to those in **I** because of the coordination of the additional bpy ligand. There is a much smaller change in the energy of the conduction band that is derived from the Re 5d orbitals. These results demonstrate that the ligand-mediated structural transformations of $(d^0/d^{10})$-hybrid solids represent a new and convenient low-temperature approach to modulate their optical bandgap sizes toward the visible wavelengths for use with solar energy.

## Introduction

Synthetic strategies that aim at the formation of specific solid-state structures have been intensely pursued and aided by the assimilation of the rich diversity and versatility of organic ligands into inorganic metal-oxides, chalcogenides, and other chemical systems.[1] The growing family of metal-oxide/organic hybrids includes many members that have been explored for potential applications in areas such as small-molecule absorption, ion-exchange, conductivity, magnetism, and catalysis.[2,3] The synthetic strategies to target new hybrid solids typically emphasize the use of the local metal-coordination geometry, as well as the geometry and size of the ligand, to help control the structure type that forms.[4,5] For example, our group has utilized hydrothermal synthetic techniques to extend this to heterometallic-oxide/organic hybrids, such as reported in the layered rhenates $M(pzc)_2(H_2O)_xAgReO_4$ (M = Co, Ni, Cu; pzc = pyrazine-2-carboxylate)[6,7] and $MReO_4(pyz)$ (M = Ag, Cu; pyz = pyrazine),[8,9] and also in the layered vanadates $[Ag(L)]_4V_4O_{12} \cdot xH_2O$ (L = 4,4′-bipyridine

*To whom correspondence should be addressed. E-mail: paul_maggard@ncsu.edu. Phone: (+1) 919-515-3616. Fax: (+1) 919-515-5079.

(1) (a) Carlucci, L.; Ciani, G.; Proserpio, D. M.; Sironi, A. *Chem. Commun.* **1996**, 1393. (b) Blake, A. J.; Champness, N. R.; Chung, S. S. M.; Li, W.; Schroder, M. *Chem. Commun.* **1997**, 1005. (c) Hagrman, P. J.; Hagraman, D.; Zubieta, J. *Angew. Chem., Int. Ed.* **1999**, *38*, 2638–2684. (d) Lin, J.; Xu, Y.; Qiu, L.; Zang, S.; Lu, C.; Duan, C.; Li, Y.; Gao, S.; Meng, Q. *Chem. Commun.* **2008**, 2659.

(2) (a) Müller, A.; Reuter, H.; Dillinger, S. *Angew. Chem., Int. Ed. Engl.* **1995**, *34*, 2328. (b) Yaghi, O. M. *Nature* **1999**, *402*, 276. (c) Yaghi, O. M. *J. Am. Chem. Soc.* **1998**, *120*, 8571. (d) Cheetham, A. M. *Science* **1994**, *264*, 794. (e) Pope, M. T.; Müller, A. *Angew. Chem., Int. Ed. Engl.* **1991**, *30*, 34.

(3) (a) Maggard, P. A.; Boyle, P. D. *Inorg. Chem.* **2003**, *42*, 4250–4252. (b) Luo, J.; Alexander, B.; Wagner, T. R.; Maggard, P. A. *Inorg. Chem.* **2004**, *43*, 5537–5542. (c) Shu, M.; Tu, C.; Xu, W.; Jin, H.; Sun, J. *Cryst. Growth Des.* **2006**, *6*, 1890–1896. (d) Niu, J.; Ma, P.; Niu, H.; Li, J.; Zhao, J.; Song, Y.; Wang, J. *Chem.—Eur. J.* **2007**, *13*, 8739–8748. (e) Yan, B.; Maggard, P. A. *Inorg. Chem.* **2007**, *46*, 6640–6646.

(4) (a) Moulton, B.; Zaworotko, M. J. *Chem. Rev.* **2001**, *101*, 1629. (b) Gimeno, N.; Vilar, R. *Coord. Chem. Rev.* **2006**, *250*, 3161. (c) Kitagawa, S.; Kitaura, R.; Noro, S.-I. *Angew. Chem., Int. Ed.* **2004**, *43*, 2334.

(5) (a) Zheng, L.; Whitfield, T.; Jacobson, A. J.; et al. *Angew. Chem., Int. Ed.* **2000**, *39*, 4528. (b) Hagrman, P. J.; Finn, R. C.; Zubieta, J. *J. Solid State Sci.* **2001**, *3*, 745–774. (c) Xu, L.; Qin, C.; Wang, X. L.; Wei, Y. G.; Wang, E. B. *Inorg. Chem.* **2003**, *42*, 7342. (d) Kong, Z.; Weng, L.; Tan, D.; et al. *Inorg. Chem.* **2004**, *43*, 5676–5680.

(6) Maggard, P. A.; Yan, B.; Luo, J. *Angew. Chem., Int. Ed.* **2004**, *44*, 2553–2556.

(7) Yan, B.; Capracotta, M. D.; Maggard, P. A. *Inorg. Chem.* **2005**, *44*, 6509–6511.

(8) Lin, H.; Yan, B.; Boyle, P. D.; Maggard, P. A. *J. Solid State Chem.* **2006**, *179*, 217–225.

(9) Lin, H.; Maggard, P. A. *Inorg. Chem.* **2007**, *46*, 1283–1290.

 Published on Web 07/13/2009 © 2009 American Chemical Society

or 1,2-bis(4-pyridyl)-ethane).[10] The latter vanadates were the first known hybrid solids to have been found to exhibit photocatalytic activity under visible-light irradiation. Thus, this research into hybrid solids primarily aims at the ligand-mediated control over the structures of metal oxides, and thus which can serve as a tool for understanding the relationship between hybrid structures and their bandgap sizes and photocatalytic activity.

Currently, an emerging route to obtain small visible-light bandgaps (i.e., ~1.5−3.0 eV) is based on incorporating mixed $d^0$ and $d^{10}$ transition-metal combinations within hybrid solids, and which results in a higher energy valence band consisting of the $d^{10}$ metal orbitals and/or the ligand-based $\pi$ orbitals.[10] For example, it has previously been shown that the absorption edge of $AgReO_4$ (3.7 eV) is shifted to lower visible-light energies via incorporation of the pyz (= pyrazine) ligand into its structure, as observed in the pillared-structure $Ag(pyz)ReO_4$ (2.9 eV).[8] However, much smaller visible-light bandgaps can be obtained by replacing $Ag^+$ with $Cu^+$ in these heterometallic hybrid solids, owing to the relatively higher-energy d orbitals of $Cu^+$. The $Cu_3ReO_4(q6c)_2$ (q6c = quinoline-6-carboxylate), $Cu(pyz)ReO_4$, and $Cu(pyz)_{0.5}ReO_4$ and $CuReO_4$ solids each exhibit an optical bandgap size within the narrow range of ~2.1−2.2 eV.[9] In the $Cu^+$-containing examples, the introduction of ligand-based $\pi$ orbitals has a negligible effect on the bandgap size because the higher energy Cu 3d-orbitals primarily form the valence band rather than the ligand-based orbitals. Thus, for $Cu^I/Re^{VII}$-oxide hybrids, there are no prior examples of using ligand-mediated tuning of the structure to influence the bandgap size.

The structural flexibility of many types of hybrid solids has enabled investigations into new low-temperature structural transformations arising from the removal or insertion of guest molecules and ligands.[11] These structural transformations have been primarily limited to the guest-exchange abilities of the hybrid structure and to its expansion or collapse, such as in the reversible absorption/desorption of coordinated water molecules in the layered molybdate and rhenate frameworks in $[M_2(pzc)_2(H_2O)_x][Mo_5O_{16}]$ (M = Co, Ni; pzc = pyrazinecarboxylate) and $M(pyz)_2(H_2O)_xAgReO_4$ (pyz = pyrazine).[12,6,7] Structural interconversions between hybrid solids are also quite limited to small guest molecules (e.g., water and methanol).[11] The structural conversion of a hybrid to a condensed metal-oxide is often possible, such as in the $MReO_4(pyz)$ (M = Ag, Cu) hybrids that exhibit layered structures containing ligands that are easily removed (irreversibly) to produce $MReO_4$.[7,9] However, the reversible insertion or removal of organic ligands within hybrid metal-oxide/organic solids is not well explored. By contrast, reversible structural transformations involving the insertion of organic ligands have been found for many solid-state coordination polymers, such as those involving a 1D → 2D or 0D → 2D structural transformation.[11] Thus, we have investigated the use of the longer bridging ligand bpy (= 4,4′-bipyridine) in the $Cu^I/Re^{VII}$-oxide system to prepare new hybrid structures and also for the ligand-mediated control over their structures and bandgap sizes.

Herein we report the hydrothermal syntheses of two new $Cu^I/Re^{VII}$-oxide hybrid solids, $Cu(bpy)ReO_4$ (**I**) and $Cu(bpy)_2ReO_4\cdot 0.5H_2O$ (**II**), and the reversible structural interconversion between them via the insertion or removal of one bpy ligand and solvent water per formula. These hybrids illustrate a unique ligand-mediated structural transformation between multiply interpenetrating frameworks, from a pillared-layered structure that is 2-fold interpenetrating in **I** to a diamond-type framework that is 4-fold interpenetrating in **II**. The accompanying changes in their optical absorption edges are analyzed with respect to their atomic and electronic structures to understand the role of the bpy ligand on the structure and bandgap sizes.

## Experimental Section

**Materials.** All starting materials were purchased commercially and used without further purification: $Cu_2O$ (99% metal basis, Alfa Aesar), $Cu(CN)_2$ (99.9%, Alfa Aesar), $Re_2O_7$ (99.9+%, Alfa Aesar), and 4,4′-bipyridine (98%, Alfa Aesar). A reagent amount of deionized water was also used in the syntheses.

**Synthesis.** The initial synthesis of $Cu(bpy)ReO_4$ (**I**) was performed by adding 28.8 mg (0.20 mmol) of $Cu_2O$, 96.8 mg (0.20 mmol) of $Re_2O_7$, 62.4 mg (0.40 mmol) of bpy, and 0.40 g (22.2 mmol) of $H_2O$ to an FEP Teflon pouch. The pouch was heat-sealed and placed inside a 45 mL Teflon-lined stainless steel reaction vessel which was backfilled with ~15 mL of deionized $H_2O$ before closing. The reaction vessel was heated to 150 °C for 72 h inside a convection oven and slowly cooled to room temperature at 6 °C/h. Pale-yellow platelet crystals of **I** suitable for single-crystal X-ray diffraction were obtained in ~50% yield based on Cu. However, the highest yields (~85%) and purities were found when reacting 23.1 mg (0.20 mmol) of $Cu(CN)_2$, 96.8 mg (0.20 mmol) of $Re_2O_7$, 31.2 mg (0.20 mmol) of bpy, and 0.40 g (22.2 mmol) of $H_2O$ at 220 °C for 5 days. The excess $Re_2O_7$ used in the reaction can be precipitated as $AgReO_4$ from the final acidic solution (pH ~2−3) by adding $AgNO_3$.

The synthesis of $Cu(bpy)_2ReO_4\cdot 0.5H_2O$ (**II**) was initially discovered by reacting the yellow product crystals of $Cu(bpy)ReO_4$ (**I**) with additional amounts of bpy ligand (1:1 ratio) in aqueous solution at 100−150 °C for 72 h (yield of ~90%), as shown in Scheme 1. The optimum synthetic procedures for the growth of larger red-block crystals of **II** were similar to that of **I** described above and using the same starting materials, with the exception of adjusting the $Cu(CN)_2$/bpy ratio to 1:2. The hydrothermal reaction was heated to 220 °C for 5 days with a yield ~95% based on Cu. Each hybrid solid was obtained in high phase purity (~100%) according to powder X-ray diffraction data (see Supporting Information) and TGA results (see below).

**Crystallographic Structure Determination.** Single-crystal X-ray diffraction data for **I** and **II** were collected on a Bruker-Nonius X8 Apex2 CCD diffractometer at a temperature of 173 K using Mo Kα. radiation ($\lambda = 0.71073$ Å). The samples were mounted on a nylon loop with a small amount of NVH immersion oil. The frame integrations were performed using the SAINT program.[13] The resulting raw data were scaled and absorption corrected using a multiscan averaging of symmetry equivalent data using the SADABS program.[14] Both structures were initially found by direct methods using the SIR92 program.[15] The hydrogen atoms

(10) Lin, H.; Maggard, P. A. *Inorg. Chem.* **2008**, *47*, 8044–8052.
(11) (a) Suh, M. P.; Ko, J. W.; Choi, H. J. *J. Am. Chem. Soc.* **2002**, *124*, 10976–10977. (b) Ohmori, O.; Kawano, M.; Fujita, M. *J. Am. Chem. Soc.* **2004**, *126*, 16292–16293. (c) Maji, T. K.; Mostafa, G.; Matsuda, R.; Kitagawa, S. *J. Am. Chem. Soc.* **2005**, *127*, 17152–17153. (d) Vittal, J. J. *Coord. Chem. Rev.* **2007**, *251*, 1781–179. (e) Bradshaw, D.; Warren, J. E.; Rosseinsky, M. J. *Science* **2007**, *315*, 977–980. (f) Cheng, X. N.; Zhang, W. X.; Chen, X. M. *J. Am. Chem. Soc.* **2007**, *129*, 15738–15739. (g) Kaneko, W.; Ohba, M.; Kitagawa, S. *J. Am. Chem. Soc.* **2007**, *129*, 13706–13712.
(12) Yan, B.; Maggard, P. A. *Inorg. Chem.* **2006**, *45*, 4721–4727.
(13) *SAINT+*, version 7.34A; Bruker-Nonius: Madison, WI, 2006.
(14) *SADABS*, version 2.10; Bruker-Nonius: Madison, WI, 2004.
(15) Altomare, A.; Cascarano, G.; Giacovazzo, C.; Guagliardi, A.; Burla, M. C.; Polidori, G.; Camalli, M. *J. Appl. Crystallogr.* **1994**, *27*, 435.

**Scheme 1.** Synthesis of **I** (left) and **II** (right) and the Structural Interconversion of Their Multiply-Interpenetrating Frameworks via a Modification of the Local Coordination Environment around Cu As a Function of the Ligand Stoichiometry[a]

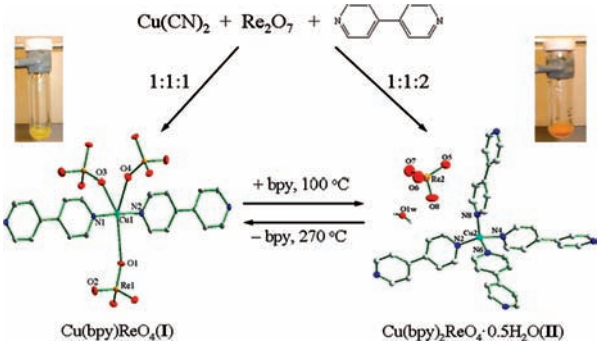


[a] Ellipsoids are drawn at the 50% probability level and all H atoms on the ligands are omitted for clarity.

**Table 1.** Selected Crystal Data and Structural Refinement Details for **I** and **II**

| | **I** | **II** |
|---|---|---|
| formula | $C_{10}H_8CuN_2O_4Re$ | $C_{40}H_{34}Cu_2N_8O_9Re_2$ |
| crystal system | orthorhombic | triclinic |
| space group, $Z$ | *Pbca*, 8 | $P\bar{1}$, 2 |
| temperature, K | 173 | 173 |
| $a$, Å | 10.8513(3) | 11.8190(4) |
| $b$, Å | 12.9419(4) | 12.6741(4) |
| $c$, Å | 15.6976(5) | 13.7585(4) |
| α, deg | 90.0 | 85.8653(13) |
| $\beta$, deg | 90.0 | 81.6197(13) |
| $\gamma$, deg | 90.0 | 84.0945(14) |
| V, Å$^3$ | 2204.52(12) | 2024.71(11) |
| $\rho$, g/cm | 2.832 | 2.084 |
| $\mu$, mm$^{-1}$ | 12.91 | 7.07 |
| reflections(total), $R_{int}$ | 48991, 0.056 | 54349,0.022 |
| data/restraints/parameters | 3753/0/163 | 11926/0/541 |
| R1, wR2[a][$I > 2\sigma(I)$] | 0.058, 0.067 | 0.035, 0.047 |

[a] $R_1 = \sum||F_o| - |F_c||/\sum|F_o|$; $wR2 = [\sum w(F_o^2 - F_c^2)^2/\sum w(F_o^2)^2]^{1/2}$; $w = \sigma_F^{-2}$.

were introduced at idealized positions and were allowed to ride on the parent carbon atoms. Next, the structural model was fit to the data using the full-matrix least-squares method based on $F$ within the LSTSQ program from NRCVAX.[16] The final structural analyses and refinement details of **I** and **II** are summarized in Table 1. The interatomic distances and angles for nearest-neighbor atom pairs are listed in Table 2. A more complete list of the structure refinement parameters can be found in the Supporting Information.

**Thermogravimetric Analyses (TGA).** Weighed amounts (~20 mg) of each compound were loaded onto Pt pans, equilibrated and tarred at room temperature on a TA Instrument TGA Q50, and the data plotted as the % starting weight versus temperature (°C). The samples were heated to 550 or 270 °C at a rate of 5 °C/min under flowing nitrogen gas (40 mL/min). Post-TGA residuals were characterized by powder X-ray diffraction in transmission mode on an Inel XRG 3000 diffractometer fitted with a CPS 120 position sensitive detector and using Cu K$\alpha_1$ radiation from a sealed tube X-ray source.

**Optical Properties.** The UV−vis diffuse reflectance spectra of the powdered samples were measured on a Shimadzu UV-3600 UV−Vis−NIR Spectrophotometer equipped with an integrating sphere. Roughly 10 mg of each sample was mounted onto a pressed $BaSO_4$ powder holder and placed along the external window. A pressed $BaSO_4$ powder was used as a reference, and the data were plotted as the remission function $F(R_\infty) = (1 - R_\infty)^2/(2R_\infty)$, where $R$ is diffuse reflectance based on the Kubelka−Monk theory of diffuse reflectance.

**Table 2.** Selected Interatomic Distances (Å) and Bond Valence Sums[a] in **I** and **II**

| atom1 | atom2 | distance (Å) | atom1 | atom2 | distance (Å) |
|---|---|---|---|---|---|
| | | **I** | | | |
| Cu1 | O1 | 3.195(4) | Re1 | O1 | 1.727(4) |
| | O3 | 2.812(4) | | O2 | 1.744(6) |
| | O4 | 2.883(4) | | O3 | 1.730(4) |
| | N1 | 1.888(5) | | O4 | 1.741(4) |
| | N2 | 1.888(5) | | $\sum S_{ij}$ | 6.8 |
| | $\sum S_{ij}$ | 0.94 | | | |
| | | **II** | | | |
| Cu1 | N1 | 2.008(3) | Re1 | O1 | 1.699(4) |
| | N3 | 2.055(3) | | O2 | 1.721(3) |
| | N5 | 2.053(3) | | O3 | 1.712(3) |
| | N7 | 2.058(3) | | O4 | 1.712(4) |
| | $\sum S_{ij}$ | 1.1 | $\sum S_{ij}$ | | 7.2 |
| Cu2 | N2 | 2.000(3) | Re2 | O5 | 1.722(4) |
| | N4 | 2.040(3) | | O6 | 1.713(4) |
| | N6 | 2.073(3) | | O7 | 1.713(4) |
| | N8 | 2.048(3) | | O8 | 1.731(4) |
| | $\sum S_{ij}$ | 1.1 | $\sum S_{ij}$ | | 7.0 |

[a] $S_{ij} = \exp[(R_0 - R_{ij})/B]$, $B = 0.37$; $R_0 = 1.574$ Å, 1.600 Å, 1.930 Å for $Cu^I-N$, $Cu^I-O$, and $Re^{VII}-O$, respectively.[17]

**X-ray Photoelectron Spectroscopy (XPS).** The XPS spectra of **I**, **II**, $CuReO_4$, and $CuReO_4$(pyz) were recorded on a RIBER LAS-3000 spectrometer using Mg Kα monochromatized radiation ($h\nu = 1253.6$ eV). The base pressure of the sample chamber was approximately $1 \times 10^{-7}$ Torr. The diameter of the X-ray spot was set at 2−3 mm, and the sample sizes were ~1 cm square. The binding energies of the valence band structures were calibrated by setting the O 1s core-level main peaks to 531.2 eV.

## Results and Discussion

**Structural Descriptions. Cu(bpy)ReO$_4$ (I).** The structure of **I**, illustrated in Figure 1, generally consists of neutral $6^3$-net layers of "$CuReO_4$" that are bridged to neighboring layers via bpy (bpy = 4,4′-bipyridine) ligands that pillar between the Cu sites. These inorganic layers are composed of corner-shared $ReO_4$ tetrahedra and $\{CuO_3N_2\}$ trigonal bipyramids that alternate and are arranged into a $6^3$ network, as shown in Figure 1B. Each $ReO_4$ tetrahedron is bonded to three different $Cu^+$ atoms in the layer via three O vertices (Cu−O distances of 2.812(4)−3.195(4) Å), with the fourth O vertex oriented either above or below the layer. Each $Cu^+$ atom is also surrounded by three oxide groups from the three separate $ReO_4$ tetrahedra, and also to the nitrogen groups on two bpy ligands oriented above and below each layer at a Cu−N distance of 1.888(5) Å. The symmetry-unique atoms are labeled in Figure 1B, and the corresponding interatomic distances are tabulated in Table 2. All near-neighbor distances are within the same range as observed in other Cu/organic hybrid solids,[3b,9] except for ionic Cu−O distances (> 2.8 Å) that are longer than typical covalent bond lengths for copper rhenates. In addition, the calculated bond valence sums ($\sum S_{ij}$) for Cu and Re, listed in Table 2,[17] are consistent with +1 and +7 oxidation states for each, respectively.

(16) Gabe, E. J.; Le Page, Y.; Charland, J. P.; Lee, F. L.; White, P. S. *J. Appl. Crystallogr.* **1989**, *22*, 384–387.

(17) Hormillosa, C. *Bond Valence Calculator*, version 2.0; McMaster University: Hamilton, Ontario, Canada, 1993.

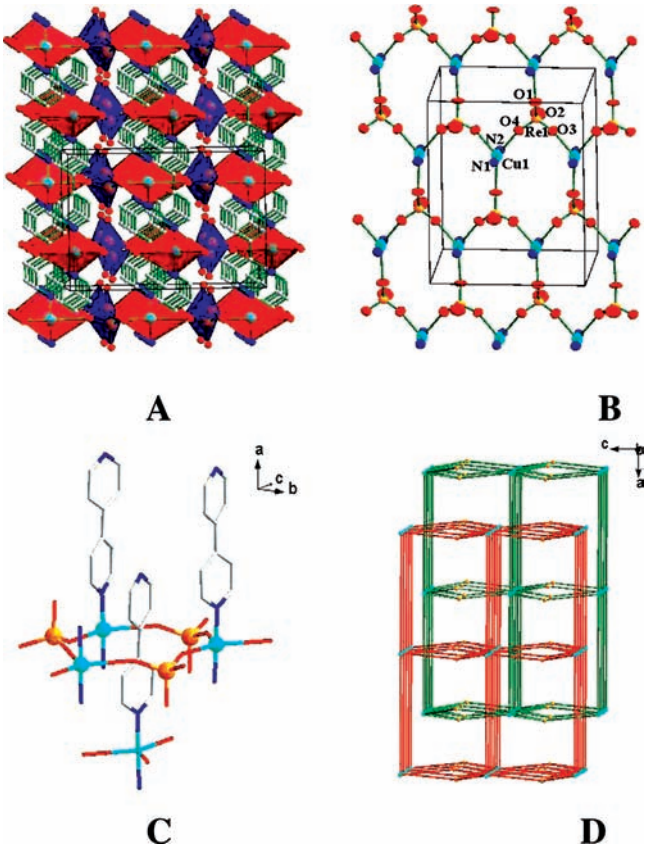


**Figure 1.** ~[010] polyhedral view of **I**, Cu(bpy)$ReO_4$ (A), red polyhedra = Cu-centered trigonal bipyramids, blue polyhedra = $ReO_4$ tetrahedra; A single "$CuReO_4$" layer (B) drawn with 80% probability thermal ellipsoids, with all symmetry-unique atom types labeled; local structural view of **I** (C) showing the interpenetration of the two frameworks, Re = yellow spheres and Cu = blue spheres; extended ball-and-stick drawing (D) of the two interpenetrating nets of **I** colored red and green, where each node represents a Cu or Re atom. All H atoms on the ligands are omitted for clarity.

The overall pillared-layered structure of **I** is roughly similar to that of Ag(bpy)$ReO_4$,[18] with the exception that **I** has two separate frameworks that are interpenetrating, as shown in Figure 1 (C and D). The two interpenetrating frameworks are related by symmetry so that there is only one symmetry-unique layer that stacks down the *a*-axis to generate the full 3D structure. A structural analysis using TOPOS[19] indicates that the interpenetrating framework of **I** represents a 3D *hms* topology (class IIa) with (3,5)-connectivity and a 2-nodal (Re, Cu) net, which is similar to that of silver coordination polymers with *hms* topology.[20,21] The total Schläfli symbol of this net is $(6^3)(6^9\cdot 8)$, and the long vertex symbol with rings is $[6\cdot 6\cdot 6\cdot 6_2\cdot 6_2\cdot 6_2\cdot 6_2\cdot 6_2\cdot *]$ $[6_3\cdot 6_3\cdot 6_3]$. The layer-to-layer distance is set by the length of the bpy ligand at 7.08 Å. However, the two pillared-layered frameworks interpenetrate through every open hexagonal window of the $6^3$ "$CuReO_4$" net, such as shown for one face in Figure 1C. Thus, the layer-to-layer distance between the two interpenetrating nets is set by half the length of the bpy ligand at ~3.54 Å. No pores are present within or between the "$CuReO_4$" layers because of the 2-fold interpenetration of the frameworks.

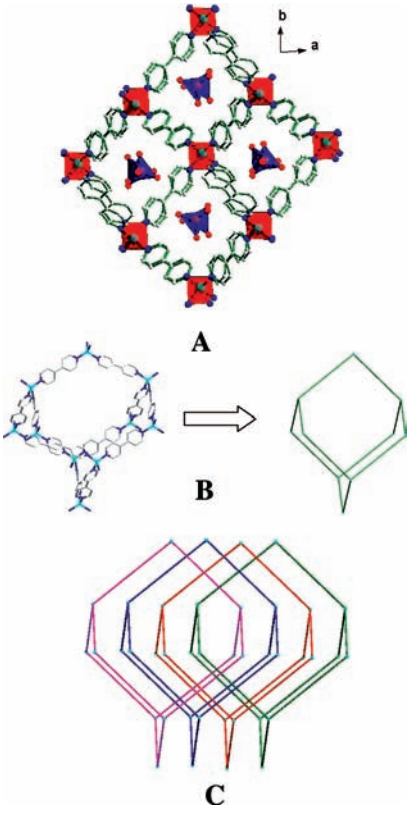


**Figure 2.** ~[001] polyhedral view of the structure of Cu(bpy)$_2$Re$O_4\cdot 0.5H_2O$ (A), **II**, with red polyhedra = Cu-centered tetrahedra and blue polyhedra = $ReO_4$ tetrahedra; a single diamond-type $Cu(bpy)_2^+$ network in **II** (B), drawn in perspective (left) and as a simplified stick model (right); a schematic representation of the four interpenetrating networks (C) in **II**, where each node represents a Cu atom. All H atoms on the ligands are omitted for clarity.

**$Cu(bpy)_2ReO_4\cdot 0.5H_2O$ (II).** The structure of **II**, shown in Figure 2, has a cubic diamond or adamantoid framework (Schläfli symbol: *dia* $6^6$, class IIIa for interpenetration) that is 4-fold interpenetrating with perrhenate $ReO_4^-$ anions and uncoordinated water molecules filling the pores. These frameworks are constructed from two symmetry-unique $Cu^+$ atoms that are each tetrahedrally coordinated by four bpy ligands, with Cu−N distances of 2.000(3) to 2.073(3) Å. There are four such independent $[Cu(bpy)_2]^+$ diamond-type networks that are interpenetrating, as shown in Figure 2 (B and C). The Cu···Cu distances from one framework to the next range from 11.11 to 11.20 Å, which allow sufficient space for three other frameworks to interpenetrate. However, a notable feature is that the interpenetrating frameworks still leave sufficient pore space to accommodate isolated $ReO_4^-$ anions between the different networks. Each of the four independent diamond-type frameworks contains channels (shortest: ~4.7 × 6.0 $Å^2$) that are oriented parallel to the [001] direction of the four frameworks, shown in Figure 2A, and that are filled with $ReO_4^-$ counterions and $H_2O$ molecules. There are two symmetry-unique $ReO_4^-$ tetrahedra with Re−O distances

(18) Lin, H.; Maggard, P. A. *Unpublished Research*, **2009**.
(19) Blatov, V. A. *TOPOS, A Multipurpose Crystallochemical Analysis with the Program Package*; Samara State University: Russia, 2004.
(20) Blatov, V. A.; Carlucci, L.; Ciani, G.; Proserpio, D. M. *CrystEngComm*. **2004**, *6*(65), 377–395. Baburin, I. A.; Blatov, V. A.; Carlucci, L.; Ciani, G.; Proserpio, D.M. *J. Solid State Chem*. **2005**, *178*, 2452–2474.
(21) Friedrichs, O. D.; O'Keeffe, M.; Yaghi, O. M. *Acta Crystallogr., Sect. A* **2003**, *A59*, 22–27.

ranging from 1.699(4)−1.731(4) Å, listed in Table 2. All interatomic distances are consistent with those in previously reported perrhenate hybrid solids.[3b,6−9] The calculated bond valence sums ($\sum S_{ij}$) for Cu and Re, listed in Table 2, are consistent with +1 and +7 oxidation states for each, respectively.

The amount of bpy ligand used in the reaction has dramatic local and long-range structural consequences on each of the crystal structures. The structure of **II** is significantly dissimilar to that observed for **I** in which a 2-fold-interpenetrating $6^3$ net framework is formed. As the bpy-ligand stoichiometry is increased, the $Cu^+$ sites in **I** change from a distorted trigonal-bipyramidal $\{CuO_3N_2\}$ coordination geometry to a tetrahedral $\{CuN_4\}$coordination geometry in **II** in which the coordinating perrhenate anions are displaced, as shown in Scheme 1. The result is a structural conversion of **I**, containing pillared layers of "$CuReO_4$", to **II** that has $Cu(bpy)_2^+$ diamond networks but no extended inorganic layers. These two structures are related to those of $[Cu(bpy)_{1.5}](NO_3)\cdot 1.25H_2O$, $[Cu(bpy)_2](NO_3)$, and $[Cu(bpy)_2](PF_6)$.[22−24] In the latter two structures, the higher bpy content results in four interpenetrating $Cu(bpy)_2^+$ diamond-like frameworks, while the former structure contains a trigonal $\{CuN_3\}$ coordination geometry with six interpenetrating networks. The results described herein indicate that the different structural preferences of these systems are primarily controlled through the bpy-ligand stoichiometry via the resultant changes in the coordination geometry of $Cu^+$.

**Ligand Mediated Interconversion of Hybrid Structures.** Metal-oxide/organic hybrid solids serve to incorporate the broad structural diversity and functionality of organic ligands into metal oxides, thereby achieving new structural topologies and physical properties. However, the ligand-mediated control over the metal-oxide structural features is nearly always investigated by reactions involving only the most basic inorganic reagents.[6−11] Less well explored is the utilization of hybrid solids themselves as intermediates for subsequent reactions yielding more complex structures, such as by incorporating additional ligands to modify the chemical composition and structure. The relatively similar chemical compositions for **I** and **II**, as well as their open-framework structures, suggested they could be amenable to low-temperature transformation reactions.

The bulk crystalline samples of **I** and **II** were characterized by Powder X-ray Diffraction (PXRD), as shown in Figure 3. PXRD data for the hydrothermally prepared samples, Figure 3 (b and e), were both in excellent agreement with the calculated diffraction patterns from the single-crystal refinement data, Figure 3 (a and d). Next, the structural transformation of the yellow crystals of **I** into the reddish-colored crystals of **II** was achieved by reacting them with 1 equiv of the bpy ligand in aqueous media at 100−150 °C for 1−3 days. A gradual but significant change of color was observed, shown in Scheme 1, that finally yielded orangish-red crystals that exhibited the PXRD patterns shown in Figure 3c. The PXRD data of this sample matched up very closely to that for the calculated

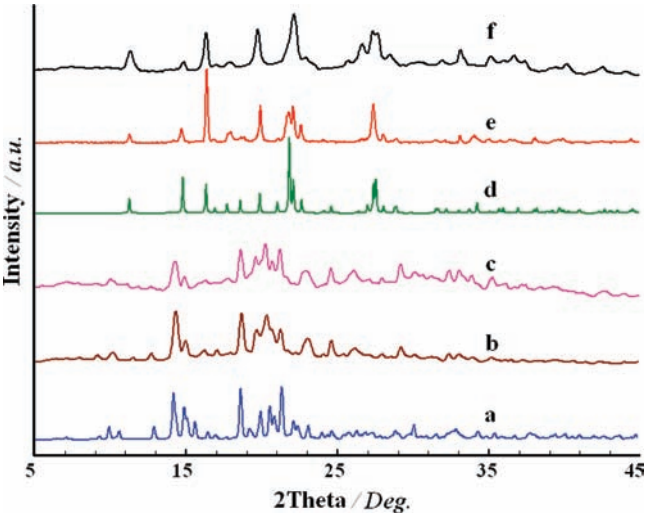


**Figure 3.** Powder XRD patterns (a) calculated from the single-crystal X-ray data of **II**, (b) of the as-synthesized crystalline sample of **II**, (c) after the reaction of **I** and bpy in water at 150 °C for 72 h, (d) calculated from the single-crystal X-ray data of **I**, (e) of the as-synthesized crystalline sample of **I**, (f) after heating **II** to 270 °C for ∼10−20 min under flowing $N_2$ gas.

and experimental patterns of **II**. These data demonstrate that the structure of **I** can be transformed into the structure of **II** via the insertion of one bpy ligand into its pillared layered structure and yielding the 4-fold-interpenetrating diamond-type topology. The interconversion of multiply interpenetrating frameworks is previously unknown in hybrid metal-oxide/organic systems, and there is only one such example known for coordination polymers.[25]

Previous research has shown that ligand removal from hybrid solids can be carried out by heating them to relatively low temperatures of ∼100−300 °C. Most often, the resultant phases are found with the removal of all organic ligands from the structure, thereby generating a new or known condensed metal oxide. Very interestingly, the crystals of **II** can be converted back into **I** by heating them to 270 °C for 10−20 min, shown in Figure 3f. The result is the removal of only one-half of the coordinated bpy ligands (and all water molecules) per formula. The crystal color also changes from red to yellow in the process. These results are significant in that **II** did not fully collapse into a condensed oxide, but instead transformed to the lower 2-fold-interpenetrating framework of **I**.

Thermal Gravimetric Analysis (TGA) was used to follow the entire thermal decomposition pathway of both **I** and **II** by heating each sample to 550 °C under flowing $N_2$ gas. The results of the TGA of **I**, shown in Figure 4, show that the structure is thermally stable to ligand loss at up to ∼300 °C, and which is followed by a large weight loss of ∼44% from ∼300 to 550 °C. This weight loss is significantly greater than that expected for the loss of bpy alone (calcd 33%). However, previous research on layered vanadates has shown that ligand removal can sometimes proceed by oxidation of the ligand and reduction of the structure via the removal of oxygen.[3e,26] A PXRD pattern of the black residue contained both $Cu_2O$

(22) Yaghi, O. M.; Li, H. *J. Am. Chem. Soc.* **1995**, *117*, 10401–10402.
(23) MacGillivary, L. R.; Subramanian, S.; Zaworotko, M. J. *J. Chem. Soc., Chem. Commun.* **1994**, 1325.
(24) Pedireddi, V. R.; Shimpi, M. R.; Yakhmi, J. V. *Macromol. Symp.* **2006**, *241*, 83–87.
(25) Zhang, J.-P.; Lin, Y.-Y.; Zhang, W.-X.; Chen, X.-M. *J. Am. Chem. Soc.* **2005**, *127*, 14162–14163.
(26) Yan, B.; Luo, J.; Greedan, J. E.; Maggard, P. A. *Inorg. Chem.* **2006**, *45*, 5109–5118.

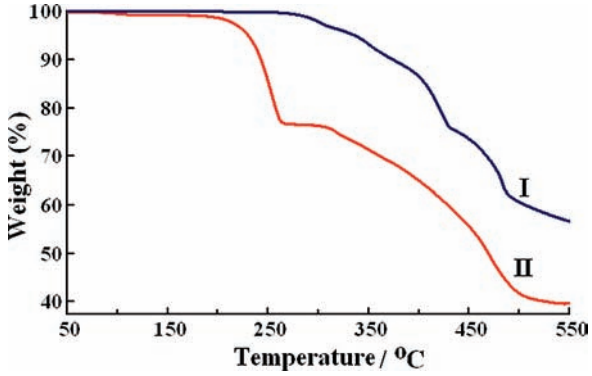


**Figure 4.** Thermogravimetric analysis (TGA) data of **I** and **II** plotted as weight (%) versus temperature (°C).

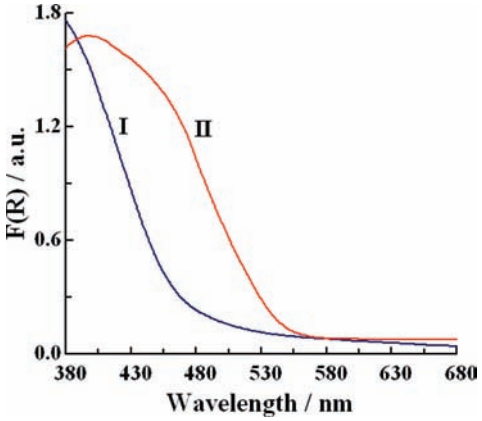


**Figure 5.** UV−vis diffuse reflectance spectra of **I** and **II**, plotted as $F(R)$ vs wavelength (nm).

and unknown rhenium-containing phases, indicating that the fully collapsed structure of **I** leads to the loss of all bpy ligands and partial loss of $\sim^3/_4$ oxygen atoms per formula. By contrast, the TGA result for **II** showed three distinct weight-loss steps. The first weight loss of ~1.5% occurred at ~200 °C and corresponded to the loss of one-half of a water molecule per formula (calcd 1.4%). The PXRD confirms that the structure of **II** has been maintained after this first weight loss owing to the removal of the lattice water, and which is possible at just 150 °C after several hours. The second weight-loss step of ~23.8% occurred between 200 and 270 °C, and matches with that expected from the removal of one bpy ligand per formula (calcd 24.6%). Further, the PXRD pattern of the yellow residue after the second weight-loss step was a close match with that of **I**, analogous to that discussed above when heating **II** to 270 °C. The data confirm that the loss of the water contained in the pores of **II** precedes the loss of the bpy ligand and the partial-condensation of the structure to give the yellow crystals of **I**. The last weight-loss step of ~36% between 300 and 550 °C shows the full collapse of the structure with the loss of the other bpy ligand and a few oxygen atoms per formula, similar to that already described for **I**. However, as shown in Scheme 1, the reversible interconversion between **I** and **II**, involving the insertion and removal one bpy ligand and one-half water molecule per formula, could be cycled back and forth numerous times. Accordingly, the reversible change in framework structures between **I** and **II** suggests that the interpenetrating $Cu^{I}/Re^{VII}$-oxide networks with bpy ligands are quite flexible and dynamic.

**Optical Properties and Electronic Structures.** Recent research has demonstrated that heterometallic hybrids containing transition metals with $d^0$ and $d^{10}$ electron configurations can exhibit small bandgap sizes with visible-light absorption that can be used to drive photocatalytic reactions.[9,10] Thus, in the synthesis of both **I** and **II** the electronic configurations were targeted to be $d^0$ for $Re^{7+}$ and $d^{10}$ for $Cu^+$. UV−vis diffuse reflectance spectra were taken of pure powdered samples of **I** and **II** to understand the influence of their different structures on their colors and bandgap absorption energies. Shown in Figure 5, the optical band gaps of **I** and **II** were estimated from the onsets of absorption edges to be ~2.5 eV and ~2.2 eV, respectively. These bandgap sizes are significantly smaller than in the related silver-containing versions of Ag(bpy)$ReO_4$ (3.5 eV) and Ag(pyz)$ReO_4$ (pyz = pyrazine, 2.9 eV), and which arises from the replacement of the lower-energy d orbitals of $Ag^+$ for the higher-energy d orbitals of $Cu^+$. However, the bandgap size of **I** is also ~0.3 eV larger than that of Cu(pyz)$ReO_4$ (2.2 eV). As has been described for Ag(bpy)$ReO_4$ and Ag(pyz)$ReO_4$, hybrid solids containing pyz ligands typically have a smaller bandgap size owing to its higher energy $\pi$ orbitals.[9] By contrast, the bandgap size of **II** is smaller or nearly the same to that found previously for Cu(pyz)$ReO_4$. Further, the XPS spectra of both **I** and **II**, shown in Figure 6, confirm that the valence orbitals in **I** are shifted to a higher binding energy by ~0.6 eV compared to that in **II**. The valence band energy of **II** is nearly the same as for the condensed $CuReO_4$, and slightly higher than Cu(pyz)$ReO_4$, and they all also share nearly the same bandgap sizes in the range of ~2.1−2.2 eV.

To understand how the change in bpy composition affects the bandgap size, the electronic structures of **I** and **II** were calculated within the Extended Hückel approach.[27] Shown in Figure 7 is the calculated electronic Densities-Of-States (DOS) for **I** and **II**, and which is overlaid with the partial DOS contribution from each constituent atom type. The electron-density contour maps for the lowest unoccupied molecular orbital (LUMO) and highest occupied molecular orbital (HOMO) of **I** and **II** are shown in Figure 8. In both structures, the lowest unoccupied orbitals (i.e., the bottom of the conduction band) were mainly formed by the Re 5d and O 2p orbitals (more minimally), as seen in the PDOS in Figure 7 and in the local orbital pictures in Figure 8. The highest occupied orbitals (i.e., the top of the valence band) consist of only the Cu 3d and N 2p orbitals in both **I** and **II**. The O 2p orbitals were not found to contribute to the valence band of either structures owing to the ionic Cu−O interactions in **I** (at > 2.8 Å) and to the lack of any close Cu−O distances in **II**. Therefore, the optical excitation from the valence to the conduction band in both structures can be viewed as mainly a metal-to-metal charge transfer between $Cu^+$ ($3d^{10}$) and $Re^{7+}$ ($5d^0$), with moderate contributions from the ligand-based orbitals in each case. Considering only the stongly interacting bpy ligands, as the amount of bpy increases from **I** to **II** the Cu coordination environment changes from a linear {$CuN_2$} to a

(27) Whangbo, M.-H. *CAESAR*; Department of Chemistry, North Carolina State University: Raleigh, NC, 1998.

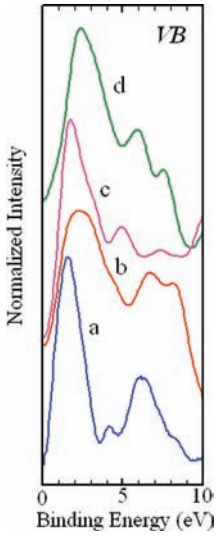


**Figure 6.** XPS valence band spectra $CuReO_4$ (a), $CuReO_4$(pyz) (b), compound **II** (c), and compound **I** (d).

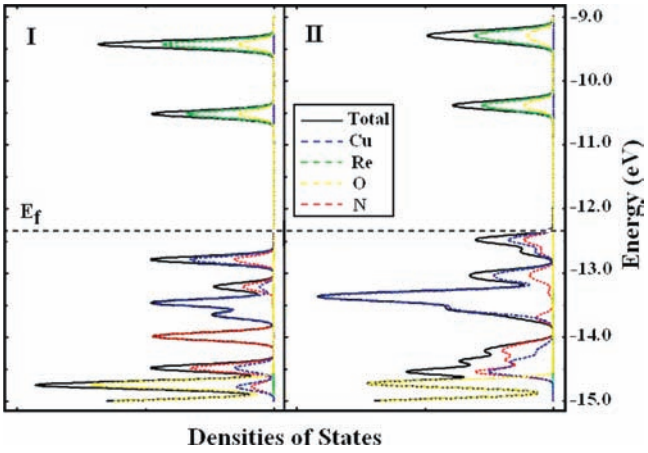


**Figure 7.** Calculated electronic DOS for **I** and **II**, with the partial DOS projected out for each atom type. The Fermi level ($E_f$) is labeled by the dashed line.

tetrahedral $\{CuN_4\}$ coordination geometry, respectively. As a result, the Cu d-orbitals in **I** are split into two sets, with $d_{z^2}$ at the highest energies. In contrast, the d-orbital splitting in **II** is separated (ideally) into two sets, the $t_2$ ($d_{xy}$, $d_{yz}$, $d_{xz}$) and e ($d_{x^2-y^2}$, $d_{z^2}$), with the former at the higher energies. Therefore the highest occupied crystal orbitals of **I** consist of mostly Cu $d_{z^2}$ and N 2p orbitals, while the highest occupied crystal orbitals in **II** are primarily composed of the $d_{xy}/d_{xz}/d_{yz}$ set and the N 2p orbitals. Thus, the greater Cu-ligand orbital interactions of **II** result in its higher-energy crystal orbitals within the valence band and also in its greater band broadening compared to **I**. In **II**, the contribution of the bpy ligands (i.e., N 2p orbitals) to the valence band is therefore larger. The result of having two additional ligands is that the valence band, composed mainly of the Cu 3d orbitals, is pushed to higher energies in **II**, as shown in Figure 7. Therefore, the band gap of **II** has been decreased as a result of the additional bpy ligands. These

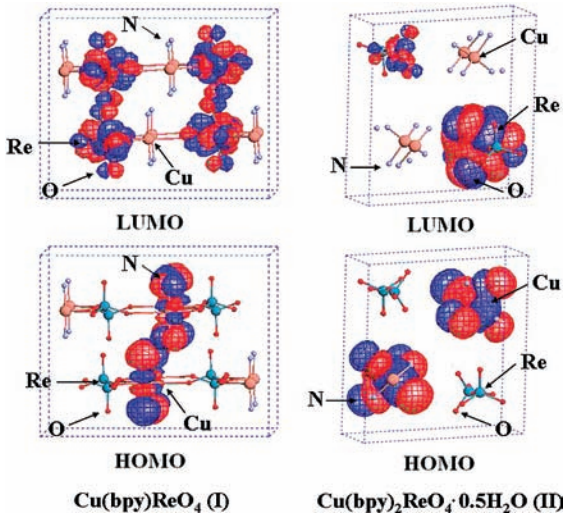


**Figure 8.** Electron-density contour maps of the LUMO and HOMO of **I** and **II**, calculated using the tight-binding method.

results show that a similar approach in other hybrid solids, focusing on the orbital energies at the local metal-coordination sites, could potentially lead to the better rational design of both the structures and optical properties of photocatalytic solids for use with solar energy.

## Conclusions

Two new copper(I)-rhenate(VII) hybrid solids, Cu(bpy)$ReO_4$ (**I**) and $Cu(bpy)_2ReO_4 \cdot 0.5H_2O$ (**II**) (bpy = 4,4′-bipyridine), with 3D 2-fold *hms* (3,5) connected and 4-fold *dia* $6^6$ interpenetrating networks respectively, could be prepared using hydrothermal reactions. A new structural interconversion was observed between **I** and **II** via the insertion of one bpy ligand and one-half water molecule per formula in aqueous media at 150 °C. Conversely, the removal of a single bpy ligand and one-half water molecule per formula from **II** at 270 °C yielded the structure of **I** again. The optical bandgap sizes were ~2.5 eV for **I** and ~2.2 eV for **II**, both within the visible-light wavelengths. These results demonstrate that hybrid structures are quite flexible and dynamic, and that the tuning of the ligand stoichiometry and the coordination geometries at low temperatures is a promising approach for the rational design of new structures with interesting optical and photocatalytic properties.

**Acknowledgments.** Acknowledgment is made to the donors of the ACS-PRF (Grant #46803-AC10) and to the Chemical Sciences, Geosciences and Biosciences Division, Office of Basic Energy Sciences, Office of Science, U.S. Department of Energy (DE-FG02-07ER15914) for support of this research, and also for assistance with the collection of single crystal X-ray data (P. Boyle).

**Supporting Information Available:** Crystallographic data for both **I** and **II** in CIF format, including crystallographic details, atomic coordinates, anisotropic thermal parameters, and interatomic distances and angles. This material is available free of charge via the Internet at http://pubs.acs.org.